Thermal, Mechanical, and Fracture Properties of Copolyureas Formed by Reaction Injection Molding: Effects of Hard Segment Structure

ANTHONY J. RYAN,*,§ TODD B. BERGSTROM,† WAYNE R. WILLKOMM,‡ and CHRISTOPHER W. MACOSKO

Department of Chemical Engineering and Materials Science, University of Minnesota, Amundson Hall, 421 Washington Avenue SE, Minneapolis, Minnesota 55455

SYNOPSIS

A series of copolyureas containing 50% by weight hard segment have been formed by RIM. The hard segment structure was systematically varied to investigate the effects of urea group density, hard segment crosslinking, relative reaction rates, and to compare the properties of aromatic and aliphatic hard segment materials. In each case the soft segment was based on a 2000 molecular weight polyether diamine. The RIM materials formed ranged from flexible elastomers to brittle plastics depending on composition and were characterized by SAXS, DSC, DMA, tensile stress–strain and fracture mechanics studies. SAXS, DSC, and DMA showed that microphase separation had occurred to give materials with a non-equilibrium morphology. DMA and tensile stress–strain studies showed the small strain properties to be very sensitive to the volume fraction of glassy material whereas the ultimate properties were dependent on chemical structure of the hard segment. Fracture properties were determined using the single-edge notch technique. In most cases ductile failure occurred with $G_c > 2.5$ kJ m^{-2} and the fracture surfaces showed gross yielding and tearing. In the case of the copolyurea with the highest urea group content, brittle fracture occurred with $G_c = 0.06$ kJ m^{-2}.

INTRODUCTION

Reaction injection molding (RIM) is a method for the high-speed production of complex polymer parts directly from low viscosity monomers or oligomers. The reactants are combined by high-pressure impingement mixing. Then they fill a mold, under low pressure, where they complete reaction to give a polymer part. The formation of solid polymeric materials involves crosslinking or microphase separation, or a combination of the two phenomena, and parts can often be demolded in less than 1 min. An excellent text concerning the fundamental science and engineering of RIM has recently been published by Macosko.[1] RIM materials are generally segmented block copolymers—the most common being polyurethanes,[2,3] poly(urethane-urea)s,[4-6] polyureas,[7-11] and poly(ether-amide)s.[12] The unique combination of physical properties available from segmented block copolymers is related to their microphase separation.

RIM polyurethanes have been extensively investigated by Macosko and coworkers.[1-3] For linear model materials the factors determining final properties are: hard segment content and crystallinity; the degree of microphase separation and copolymer molar mass. Similar model studies have been made by Willkomm and coworkers[8] on linear copolyureas based on DETDA and these studies emphasize the improved physical and thermal properties of materials containing polyurea hard segments and are in general agreement with published studies of poly(urethane-urea)s.[1,4-6] The improvement in

* Present address: Manchester Materials Science Centre, University of Manchester Institute of Science and Technology, PO Box 88, Manchester M60 1QD, UK.

† Present address: Materials Science Department, Northwestern University, Evanston, IL 60208.

‡ Present address: Dow Chemical USA, Texas Division, Building B4812, Freeport, TX 77541.

§ To whom correspondence should be addressed.

Journal of Applied Polymer Science, Vol. 42, 1023–1039 (1991)
 CCC 0021-8995/91/041023-17$04.00

poly(urethane-urea) and polyurea properties compared with polyurethanes is often without the benefit of crystallinity and is due to the higher driving force to microphase separation, from both thermodynamic and hydrogen bonding considerations. Furthermore, this type of copolyurea may only be processed by RIM as their glass transition temperature is so high that melt processing is impossible. The present work studies the role of the hard segment structure for a range of materials. The effects on the thermal and mechanical properties of urea group density, relative polymerization kinetics, crosslinking, and aromaticity are investigated for 50% hard segment copolyureas.

The thermodynamics of diblock copolymer systems are complex and beyond the scope of this paper, however, a few major features will be highlighted.[13,14] Due to the competition between the enthalpy and entropy of (micro) mixing, like monomer units will begin to aggregate at some temperature to form equilibrium microstructures. This weak first order process[14] is known as the order–disorder transition, ODT, or the microphase separation transition, MST, and the composition dependent, equilibrium microstructures formed are predicted to be either a body centered cubic array of spheres in a matrix or a two dimensional, hexagonal array of rods in a matrix or alternating lamella. These structures have been observed experimentally by a number of workers.[15,16]

The thermodynamics of segmented block copolymers are not at all well understood; theoretical predictions of the MST have been established[17] but predictions of morphology are not available at present. Experimentally, microstructures similar to those found for model diblocks have been observed by microscopy.[18–20] Generally, the polydispersity (in both block length and global molecular weight) of segmented block copolymers means that imperfect microstructures form and bulk materials which pass from the bulk homogeneous (disordered) state through the MST into the ordered state are not normally at equilibrium, therefore, annealing has been observed to "improve" morphology.[20]

The formation of a linear copolyurea is shown in Scheme 1. Typically such a polymer could be formed from 4, 4′ diphenylmethane-diisocyanate, MDI, reacting with 3, 5 diethyltoluenediamine, DETDA, and an aliphatic polyether diamine (normally of 1000–4000 molar mass). A segmented block copolymer is only formed in the special case of complete reaction.[21] At low conversions, the copolyurea forming system is a mixture of unreacted aromatic-monomers, end-capped polyether and short hard segment

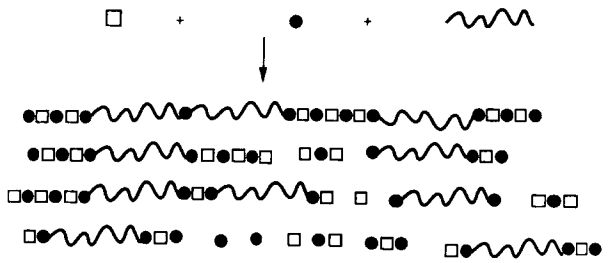

Scheme 1 Formation of a linear copolyurea. (□) short diamines; (●) diisocyanates; and (〰) macro diamines.

sequences (the aliphatic amine reacts $\sim 10^4$ times faster than the aromatic amine.[22]) At higher conversions the material will be a mixture of unreacted aromatic-monomers, hard segment sequences, and tri-, penta- . . . multiblock copolymers. The chemical reactions increase the degree of polymerization, N, and change the interaction parameter between the components, χ. The increase in the product χN has been shown[23,24] to be equivalent to a thermodynamic quench from disordered or one phase space into either the ordered (microphase separated) region of the block copolymer microphase diagram or into the unstable region of the phase diagram of the mixture. Thus a multi-block copolymer will microphase separate whereas a mixture of oligomers or polymers will macrophase separate. In either case this will be manifest *as physical gelation in a linear copolymerization* when an infinite network forms by vitrification of the hard segment rich phase. The precise nature of the phase transition in RIM materials is still unclear, i.e., micro- or macrophase separation, however, the rheological changes that accompany it have been measured.[3]

Ryan and coworkers have previously reported[23] studies on phase separation in poly(urethane-urea)s and polyureas formed by RIM and the thermodynamics of segmented block copolyurethanes, copoly(urethane-urea)s and copolyureas are reviewed in more detail in that paper. The experimental data on RIM materials were interpreted in terms of the chemical reaction during RIM polymerization causing an enormous change in the thermodynamics of the system which is analogous to a deep quench into the unstable region of the phase diagram. The existence of cocontinuous morphologies, inferred from physical properties, was interpreted as a relic of spinodal decomposition where microphase separation was arrested before reaching equilibrium by vitrification of the hard segment microphase. Ryan has also studied[24] phase separation in segmented copolyureas and poly(urethane-urea)s by the forma-

tion of model polyurea–polyether blends with no covalent bonds between the phases. The polyblends had similar thermal and small-strain mechanical properties to the analogous copolymers (their moduli are identical from 50 to 200°C). Selective extraction of 80% of the polyether phase indicated its continuity. Scanning electron micrographs of internal fracture surfaces of the remaining hard segment phase showed a random continuous structure with a wavelength of ~ 200 nm. (This is an order of magnitude larger than the size scale observed by SAXS for RIM copolyureas by Willkomm et al.[8] and is probably due to the lack of interphase covalent bonding.) Thus, this model polyurea–polyether blend had a random cocontinuous morphology which was interpreted as a relic of spinodal decomposition arrested by vitrification.

The thermal and mechanical properties of model copolyureas have been dealt with by a number of workers,[7-10,23] however, there is a paucity of information concerning the fracture properties of RIM materials. Shortall and coworkers[25,26] have studied the fracture properties of reinforced polyurethanes and Stanford[27] studied the fracture of reinforced polyurethanes by instrumented impact testing. More recently, Ryan et al.[28] reported mechanical properties studies on a well-characterized series of RIM poly(urethane-urea)s. The modulus of the polymers gave a good fit, over a wide range of composition, to a model for materials with a cocontinuous morphology. Fracture properties were investigated using the single-edged notch technique; ductile fracture occurred in low hard segment materials with critical strain energy release rates, $G_c > 6$ kJ m^{-3} and the fracture surfaces showed gross tearing, brittle fracture was observed in high hard segment materials with $G_c < 3$ kJ m^{-3}. No microstructural explanation of these phenomena was sought by these authors.

This paper reports a systematic study of the thermal, mechanical, and fracture properties of a series of copolyureas with well-defined chemistry and processing conditions. The discussion is organized into three sections which deal with the effects of urea group density, the effects of crosslinking and polymerization kinetics at constant urea-group density, and the effect of aromatic versus analogous aliphatic hard segments. Thus, the thermal, tensile stress–strain and fracture properties of the three sets of materials are compared and correlated to the microstructure, by SAXS, and the chemical structure of the reactants. To characterize the intrinsic fracture properties of these materials, we attempt to determine the critical strain energy release rate, G_c, which is a property of the material.

EXPERIMENTAL

Reactants

The materials formed in this study comprised three components: (i) a polyisocyanate, (ii) a polyether diamine soft segment oligomer, and (iii) an aromatic diamine chain extender.

The four isocyanates used were pure MDI (4,4′-diphenylmethane diisocyanate, Isonate 125M, Dow Chemical), LF-168 (uretonimine modified MDI, Rubicon LF168, ICI Americas), TDI (an 80 : 20 mixture of the 2,4 and 2,6 isomers of toluene diisocyanate, T80, Dow Chemical), and H_{12}MDI (4,4′-dicyclohexylmethane diisocyanate hydrogenated MDI, Desmondur W, Mobay).

The soft segment oligomer was D2000 (a polyoxypropylene diamine of nominal molecular weight 2000 g mol^{-1}, Jeffamine D2000, Texaco Chemical).

The four aromatic diamine chain extenders were DETDA (an 80 : 20 mixture of the 2,4– and 2,6-isomers of 3,5-diethyltoluene diamine, Ethacure 100, Ethyl Corp.), DMTDA (an 80 : 20 mixture of the 2,4- and 2,6-isomers of 3,5-dimethylthiotoluene diamine, Ethacure 300, Ethyl Corp.), MDEA (4,4′-methylene-bis(2,6-diethylaniline), Lonza), and MDECA (4,4′-methylene-bis(2,6-diethylcyclohexylamine), Lonza).

All materials were used as received and the specific polyurea formulations are shown in Table I along with the reactant structures. The polymers are referred to by the abbreviations of the reactants that form their hard segments; for example, the material formed by reacting MDI, D2000 and DETDA is referred to as MDI/DETDA. All the polymers contain 50% by weight polyether and the weight fraction of isocyanate is reported. The values of hard segment volume fraction, ϕ_{HS}, given in Table I were estimated from the calculated densities of the hard segment (according the method of van Krevelen[29]).

Reaction Injection Molding

A mini-RIM machine with lever arm control was used in this study. The machine and its operation are described in detail elsewhere.[30] Machine volume ratio was calibrated using liquid petroleum and shown to be ±0.5%. To maintain functional group stoichiometry of 1.0, at 50% by weight hard segment, the volume ratios were adjusted for each copolyurea material and these data are given in Table I. The mixhead was based on the design of Macosko and McIntyre[31] and this type of mixhead allows reactant recycle prior to impingement mixing. Polyamine Reynolds numbers were ~ 800 to ensure good mix-

Table I Reactant Structures, Formulations, and Processing Conditions[a]

Polymer	W_{iso}	R_v[b]	ϕ_{HS}	T_{mold} (°C)	t_{gel} (s)	t_{demold} (min)[c]
MDI/DETDA	0.317	2.627	0.455	110	1.3	2
MDI/DMTDA	0.298	2.755	0.441	120	8.1	5
LF168/DETDA	0.308	2.413	0.455	100	1.3	2
MDI/MDEA	0.257	3.358	0.471	75	2.5	1
H_{12}MDI/MDECA	0.260	3.120	0.502	85	3.0	1
TDI/DETDA	0.259	3.473	0.449	120	1.0	5

[a] All formulations comprise 50% by weight of the polyether diamine D2000.
[b] R_v is the ratio of the reactant volumes (isocyanate vs. diamines).
[c] Selected to give a demold time greater than the brittle to tough transition.
Reactant structures are continued below.

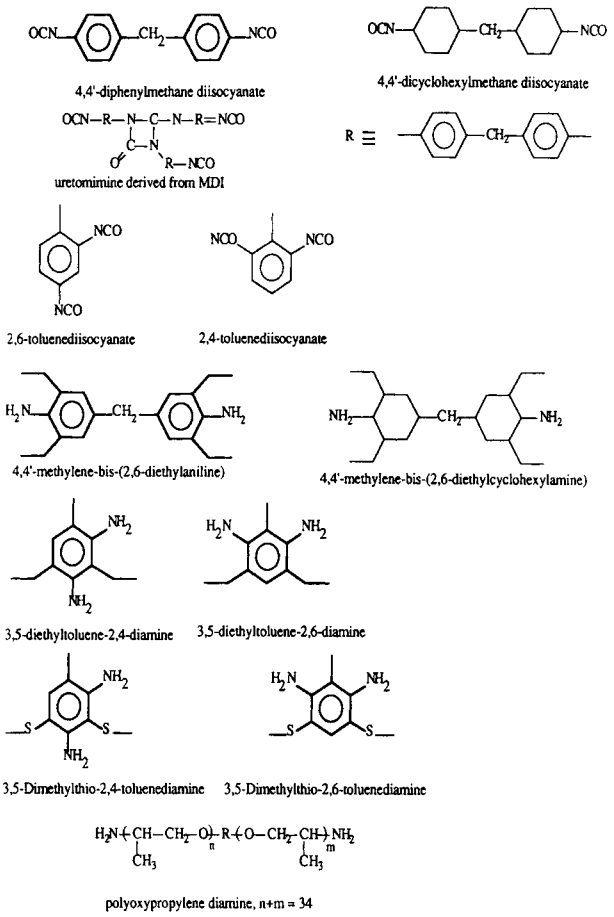

ing. Adiabatic temperature rise data[8,11] shows no polyamine Reynolds number dependence in the range 500–1000 for the MDI/DETDA system. The isocyanate Reynolds numbers were an order of magnitude greater. From the mixhead the reactive mixture passes through an aftermixer and a dam-gate assembly (ref. 1, Figs. 4.46 and 5.23) and into a rectangular cavity of dimensions 280 × 100 × 3 mm.[11]

The chain extender and D2000 were weighed, blended, degassed (at a vacuum of ~ 3 mm Hg for 18 h at 60°C) and loaded into one side of the RIM machine and the isocyanate was loaded into the other side. The tanks were then blanketed with nitrogen and the materials heated up to 60 ± 5°C. The gel-time reported in Table I was estimated by opening the mold during or shortly after filling and observing the material, the gel time obtained in this

manner was compared with the adiabatic temperature rise curves and correlated with approximately 70% conversion. The mold temperature and demolding time are reported in Table I. Molding-area diagrams were constructed for each material[8,11] and the polymers used in subsequent experiments were demolded at temperatures and times greater than that of the brittle to tough transition. (The TDI/DETDA material was always brittle on demolding.)

Polymer Characterization

The as-molded materials were characterized using small-angle X-ray scattering (SAXS), differential scanning calorimetry (DSC), dynamic mechanical analysis (DMA), and by tensile stress–strain measurements on dumbbell specimens (ASTM D 638-86) for Young's modulus, ultimate stress and ultimate strain and on notched strips for fracture mechanics analysis.

A Kratky camera with slit collimation and a one-dimensional, position sensitive detector was used in the SAXS studies. The X-ray source was a Rigaku 12 kW rotating anode operating at a potential of 105 kV and a current of 40 mA. A nickel filter gave predominantly Cu-Kα radiation of wavelength 1.542 Å. The collimation slit was 30 μm by 10 mm and the sample to detector distance was 683 mm. The Braun model OED 50 m position sensitive detector has a 10 mm platinum wire detector with a spatial resolution of $\sim$ 50 μm. The experimental data were corrected for background scattering and detector sensitivity but were not converted into units of absolute intensity. The equations used in data analysis are corrected for the effects of slit smearing so that smeared data may be used in the analysis without introducing additional noise via the desmearing process.

DSC (TA 3000, Mettler Inc.) was used for heat capacity measurements to examine the polyether glass transition temperature, T_g^s. The values of T_g^s reported are taken at the midpoint of the transition and the specific heat capacity change, ΔC_p, was determined from the endothermic displacement in the in baseline at T_g^s. The heating rate was 10°C/min and dry nitrogen was used as a purge gas with a sample mass of 10–20 mg.

DMA data were obtained in the torsion rectangular mode at 1 Hz (System IV, Rheometrics Inc.). Test bars with dimensions of 30 × 10 × 3 mm were milled from RIM plaques. Measurements were shown to be strain insensitive in the region used (1% strain) and were made in a nitrogen atmosphere at a heating rate of 2°C/min from −100 to 300°C.

Tensile stress–strain data were obtained at 23 ± 3°C on an Instron 1011 Universal Testing Machine interfaced to a Macintosh II computer through a Strawberry Tree Workbench A/D board. Dumbbell specimens (according to ASTM D638-86) having an overall length of 4.5″, a gauge length of 1″, a width of 0.25″, and a thickness of $\sim$ 1/8″ were used. The initial distance between the grips was 2.5″ and the extension rate 0.394″ min^{-1}. (The strain in the sample was calculated from the separation of the jaws of the Instron and thus the Young's modulus may be subject to an error of $\sim$ ±5% due to the whiplash in the screw drive mechanism and the anisotropic deformation of the specimen.) The tensile properties reported are the mean of at least five tests.

Fracture mechanics measurements were made on the apparatus described above, at least 20 specimens were tested for each material. The single edge notch geometry[32] used for G_c measurements was rectangular specimens of length 50 mm, width (d) 10 mm, and thickness 3 mm. Notch depths, a, were varied from 0.5 mm to 6 mm with an extension rate 10 mm min^{-1} and a gauge length of 30 mm. The onset of crack propagation was determined visually and flagged on the force–time data file. In the case of G_c measurements the strain energy density, W_c, of the specimen was determined from the integral of a third order polynomial fit to the force–time curve, between zero deflection and the point of crack propagation. For determination of K_c, the elastic stress to fracture, σ_c, of specimens with the geometry described above, was determined from the force–time curves. Fracture surfaces were coated in gold and low magnification scanning electron micrographs were obtained on an SEM 840 (Jeol, Inc.) at an accelerating voltage of 5 kV.

RESULTS

Small Angle X-Ray Scattering

The SAXS curves of the copolyureas are shown in Figure 1, the data are in the form of smoothed, smeared relative intensity, I, vs. scattering vector, q ($=(4\pi/\lambda)\sin\theta$), where λ is the wavelength of the incident radiation and θ is the scattering angle. The curves show no clear peaks and must be further analyzed to yield structural information. However, the TDI/DETDA and H_{12}MDI/MDECA systems show distinct shoulders in I vs. q which compare with length scales obtained from further analysis.

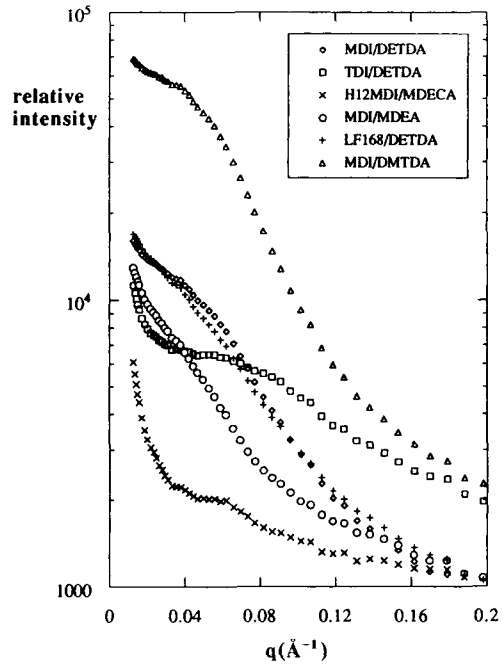

Figure 1 Smoothed, smeared SAXS curves (only 11% of each set of data points are shown for the sake of clarity).

In an attempt to obtain some information regarding the periodicity of the structure formed we assume that the material has a one-dimensionally isotropic morphology and obtain a Bragg spacing, d_1, where

$$d_1 = \lambda/2 \sin \theta_{max} = 2\pi/q_{max} \quad (1)$$

This is done by applying the Lorentz correction,[33] q^2, to the observed scattered intensity and taking the maximum of the $I(q)q^2$ vs. q plot in the calculation of d_1 in Table II.

To obtain a three-dimensional picture of a random structure Debye and Bueche[34] developed the concept of a correlation length to indicate the length scale of electron density fluctuations in an inhomogenous media. A correlation function $\gamma(r)$, relating the local fluctuations in electron density at points a and b, η_a and η_b, a distance r apart to the average value of the fluctuations for the entire sample $\langle \eta^2 \rangle$ was defined as

$$\gamma(r)\langle \eta^2 \rangle = \langle \eta_a \eta_b \rangle \quad (2)$$

where $\gamma(r)$ is 0 at large r and 1 at $r = 0$. Debye et al.[35] evaluated $\gamma(r)$ for a random two-phase system, using the probability that a rod of length r had both ends in the same or different phases and obtained an exponential form for the correlation function

$$\gamma(r) = \exp(-r/a_c) \quad (3)$$

where a_c is the correlation length. The Fourier transform of eq. (3) yields an expression for the scattered intensity which is given, after modification for slit smearing, as

$$I(q) = A/(1 + a_c^2 q^2)^{3/2} \quad (4)$$

thus a plot of $I^{-2/3}$ vs. q^2 may be used to obtain the correlation length as $a_c = [\text{slope}/\text{intercept}]^{1/2}$. The values of the correlation length presented in Table II are then used to calculate the average chord lengths through $l_{HS} = a_c/\phi_{SS}$ and $l_{SS} = a_c/\phi_{HS}$. (The SAXS data for H_{12}MDI/MDECA was not suitable for this analysis due to its low scattering power.) The value of the correlation length, a_c, obtained here for the MDI/DETDA system of 28 ± 3 Å is in agreement (within experimental error) to that of 25 Å previously obtained by Willkomm et al.[8] In each case l_{SS} is greater than the radius of gyration of the soft segment calculated to be 34 Å by Willkomm et al.[8]

Table II Thermo-Mechanical and SAXS Data for Copolyureas Formed by RIM

	DSC		DMA		SAXS			
Polymer	T_g^S (°C)	ΔC_p (J/g)	T_g^S (°C) (tan δ_{max})	$G'(-30°C)/G'(+70°C)$	d_1 (Å) (Eq. 3)	a_c (Å) (Eq. 4)	l_{SS} (Å) (a_c/ϕ_{HS})	l_{HS} (Å) (a_c/ϕ_{SS})
MDI/DETDA	−48	0.14	−45	3.7	87	28	62	51
MDI/DMTDA	−47	0.12	−53	3.8	104	34	77	61
LF168/DETDA	−47	0.13	−50	5.1	96	28	62	51
MDI/MDEA	−47	0.14	−51	3.2	126	34	72	64
H_{12}MDI/MDECA	−51	0.17	−53	2.3	87	—	—	—
TDI/DETDA	−49	0.19	−51	2.1	79	14	31	25

Differential Scanning Calorimetry

DSC was used to study the low-temperature thermal properties of the microphase-separated copolyureas and values of T_g^s and ΔC_p are presented in Table II along with the values of T_g^s from the dynamic mechanical data. All the DSC T_g values were in the range −51 to −47°C. D2000 end-capped with the stoichiometric amount of phenyl isocyanate has a T_g of −52°C under these conditions and this is in contrast to the T_g of −70°C measured for pure D2000 by Chen et al.[36] The increase in T_g, of the capped oligomer over that of the pure oligomer, is due to the loss of chain-end mobility due to hydrogen bonding as well as the incorporation of ~ 10% of aromatic material. Thus the similar values of T_g^s observed suggests that little hard segment is solubilized in the soft segment domains. The specific heat capacity change, ΔC_p, gives an indication of the degree of microphase separation (this may be calculated from the knowledge of the ΔC_p value of the pure oligomer according to the method of Camberlin and Pascault[37]) and these data have also been included in Table II. The degree of microphase separation varied from 47% for MDI/DMTDA to 74% for TDI/DETDA.

Dynamic Mechanical Analysis

The dynamic mechanical spectra of the microphase separated RIM copolyureas are presented in Figures 2–4 and the derived values of T_g^s and the modulus ratio $G'(-30°C)/G'(+70°C)$ are included in Table II. Overall, two major transitions are observed. The soft segment glass transition, T_g^s, is observed as a drop of about an order of magnitude in the storage modulus and as peaks in the loss modulus (not shown) and tan δ curves. Some of the materials also show a hard segment glass-transition temperature, T_g^H, as a definite peak in tan δ and drop in modulus followed by a modulus plateau (see, e.g., the curves for MDI/DMTDA in Fig. 3). Others show no peak in tan δ which could be associated with T_g^H and only a catastrophic drop in G' around 300°C (see, e.g., the curves for H_{12}MDI/MDECA in Fig. 4). It must be emphasized that the aromatic materials begin to degrade around this temperature and the high temperature portions of the curves are not reproducible if the material has spent significant time (> 20 min) above 250°C.

The materials whose dynamic data are presented in Figure 2 have different urea-group densities. Both TDI/DETDA (6.9 mol (—NHCOHN—) m^{-3}) and MDI/MDEA (4.0 mol (—NHCOHN—) m^{-3}) are well-phase-separated and have T_g^s values of −51°C

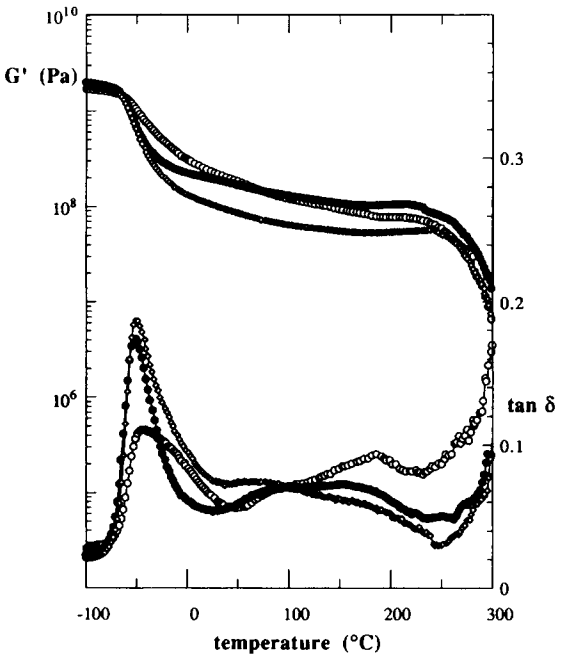

Figure 2 Dynamic shear modulus, G', and mechanical damping, tan δ, vs. temperature for copolyureas with different urea group content. (●) TDI/DETDA; (○) MDI/DETDA; and (◇) MDI/MDEA.

whereas the intermediate MDI/DETDA (5.3 mol (—NHCOHN—) m^{-3}) material has a T_g^s of −45°C and appears to be phase-mixed based on the shape of the modulus curve. Also, the peak in tan δ associated with T_g^s is much less intense for the MDI/DETDA material. The slope of the G' curve may be quantified by the modulus ratio $G'(-30°C)/G'(+70°C)$ presented in Table II and the MDI/DETDA material has the highest value for this set of materials. There appears to be a third less intense transition, indicated by a shoulder in tan δ, which occurs in the temperature interval 50–100°C for all three materials. MDI/MDEA has no peaks in tan δ above T_g^s but the modulus drops and tan δ diverges above 270°C. MDI/DETDA shows a definite peak in tan δ at ~ 180°C but there is not a corresponding drop in the storage modulus which would unambiguously indicate a T_g^H. The broad peak in tan δ between 50 and 200°C for TDI/DETDA is obviously not a T_g^H as there is very little temperature-dependence of the modulus in this region. However, TDI/DETDA does show a catastrophic drop in modulus and an asymptotic trend in tan δ above 280°C. Between 50 and 300°C the MDI/MDEA and TDI/DETDA curves are approximately parallel with a $\Delta G'$ of ~ 300 MPa, the MDI/DETDA curve joins this parallelism for a shorter interval above 200°C.

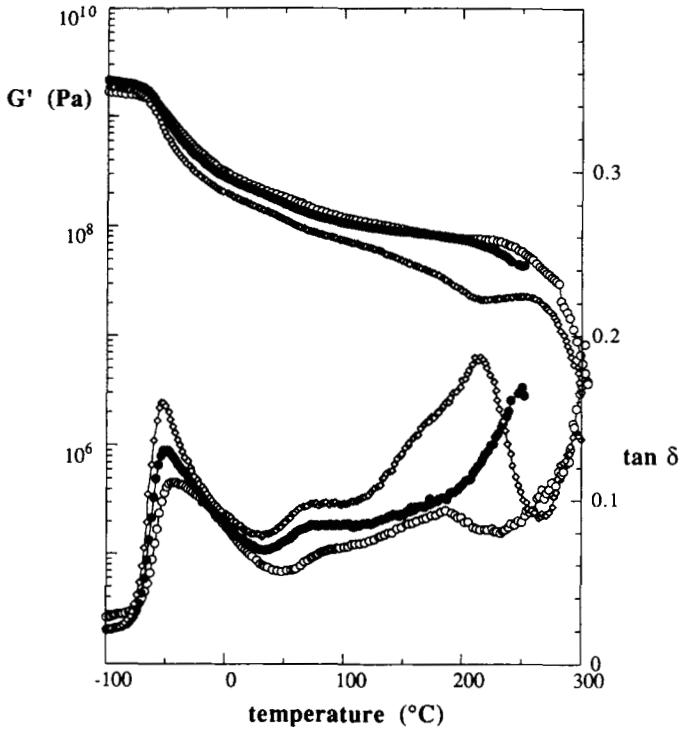

Figure 3 Dynamic shear modulus, G', and mechanical damping, tan ∂, vs. temperature for copolyureas with similar urea group content but different hard segment structure. (●) LF168/DETDA; (○) MDI/DETDA; and (◇) MDI/DMTDA.

The effect of polyurea structure on the dynamic–mechanical properties of the copolyureas with similar urea-group densities is shown in Figure 3.

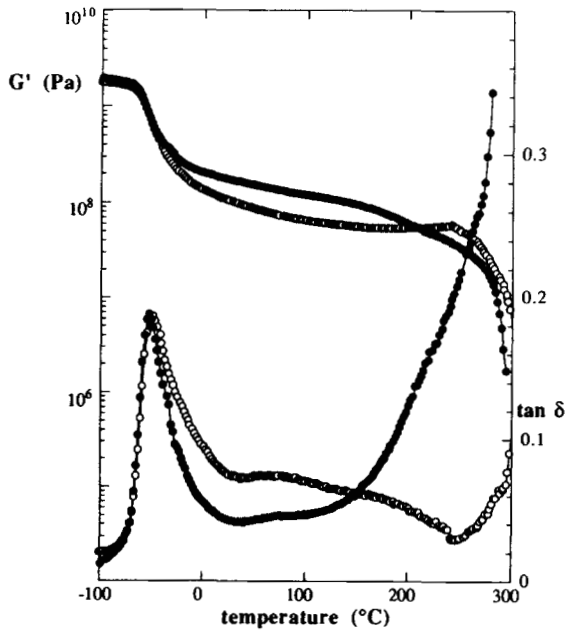

Figure 4 Dynamic shear modulus, G', and mechanical damping, tan ∂, vs. temperature for (●) H12MDI/MDECA and (○) MDI/MDEA.

LF168/DETDA has very similar behavior to MDI/DETDA with a gradual drop in G' after T_g^s leading to a modulus plateau that extends over 200°C, however, the modulus of the former falls off earlier than that of the latter. The damping behavior of these two polymers is also similar, the peak associated with T_g^s is more intense for LF168/DETDA and the mid-temperature range shoulder occurs at a lower temperature. As previously mentioned MDI/DETDA has a peak in tan ∂ at ~ 180°C and at this temperature TDI/DETDA's tan ∂ curve starts to gradually rise. The dynamic mechanical properties of the sulfur containing MDI/DMTDA both compare and contrast with those of the previously discussed materials. The location of T_g^s is essentially the same for this material and both the damping and elastic modulus behavior in the region of T_g^s and the location of the mid-temperature range shoulder are consistent with it's alkyl analogs. The high-temperature behavior of MDI/DMTDA, associated with the hard segment, contrasts strongly with its alkyl analogs. There is a definite peak in tan ∂ at 215°C and drop in modulus followed by a modulus plateau, which may be associated with a hard segment glass-transition temperature, T_g^H. However, the ultimate drop in modulus and rise in tan ∂ is similar to the other materials.

The dynamic mechanical properties of polyureas

Table III Tensile and Fracture Properties (at 23 ± 3°C) of Copolyureas Formed by RIM

Polymer	E (MPa)	σ_y (MPa)	ϵ_y (%)	σ_u (MPa)	ϵ_u (%)	G_c (kJ m^{-2})	K_c (MPa m$^{-1/2}$)	b_{min} (mm)[c]
MDI/DETDA	557	17.6	11	24.5	134	2.68[a]	1.22[b]	13.1
MDI/DMTDA	426	13.7	7	21.5	157	3.19[a]	1.16[b]	19.7
LF168/DETDA	533	17.2	9	26.7	116	3.39[a]	1.34[b]	16.5
MDI/MDEA	266	8.5	13	16.8	222	7.12[a]	1.38[b]	71.3
H_{12}MDI/MDECA	505	19.6	10	28.1	108	3.22[a]	1.27[b]	11.5
TDI/DETDA	532	15.9	5	15.3	17	0.06[b]	0.17[a]	0.3

[a] Measured value.
[b] Value calculated using eq. 7.
[c] The specimen thickness was 3 mm.

with aromatic and aliphatic hard segments are compared in Figure 4. The location of T_g^s and both the damping and elastic modulus behavior in the region of T_g^s, are essentially the same for both materials. The aliphatic material has higher G' and lower tan δ values than the aromatic material between T_g^s and 200 and 150°C respectively. H_{12}MDI/MDECA's modulus curve increases in slope and the value of tan δ begins to rise dramatically around 150°C. In the temperature interval 200 to 250°C the modulus of MDI/MDEA is rising and tan δ is small, the classical behavior of an elastic network.

Tensile Stress–Strain Studies

The results of tensile stress–strain studies are presented in Table III in the form of Young's modulus, E, yield stress, σ_y, yield strain, ϵ_y, ultimate stress (or tensile strength), σ_u, and ultimate strain (or elongation at break), ϵ_u, and representative stress–strain curves are presented in Figures 5–7. The tensile properties of MDI/DETDA were previously reported by Wilkomm.[8] Whilst the ultimate properties are in reasonable agreement the value of modulus reported here is 2.4 times greater. There is an anom-

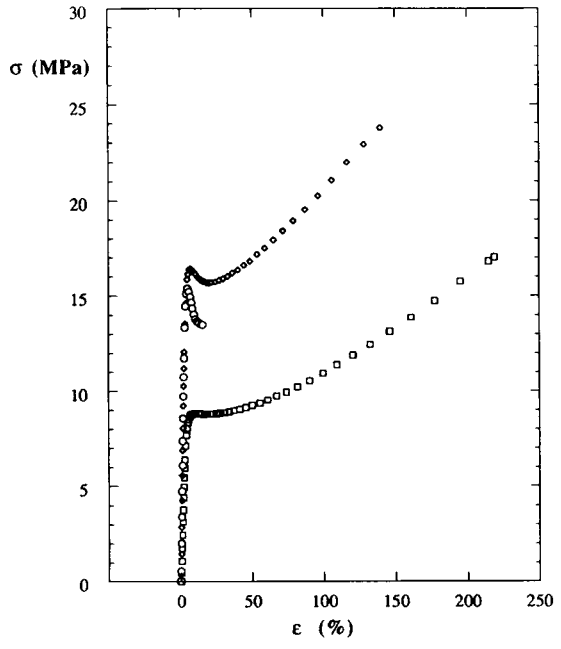

Figure 5 Representative stress–strain curves for copolyureas with different urea group content. (○) TDI/DETDA; (◇) MDI/DETDA; and (□) MDI/MDEA.

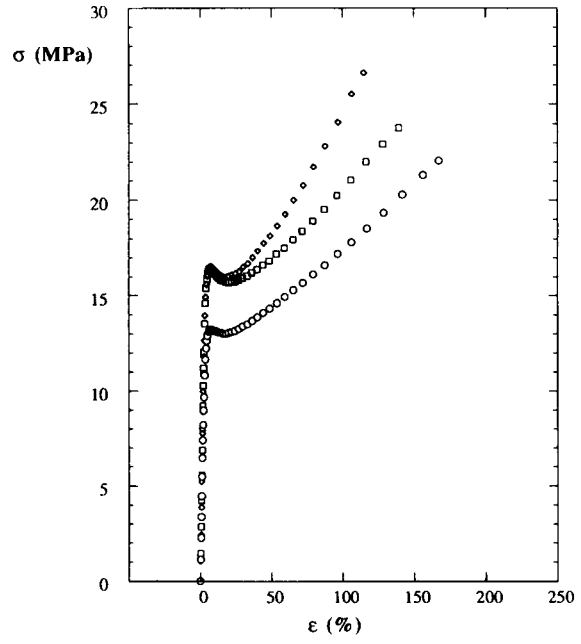

Figure 6 Representative stress–strain curves for copolyureas with similar urea group content but different hard segment structure. (◇) LF168/DETDA; (□) MDI/DETDA; and (○) MDI/DMTDA.

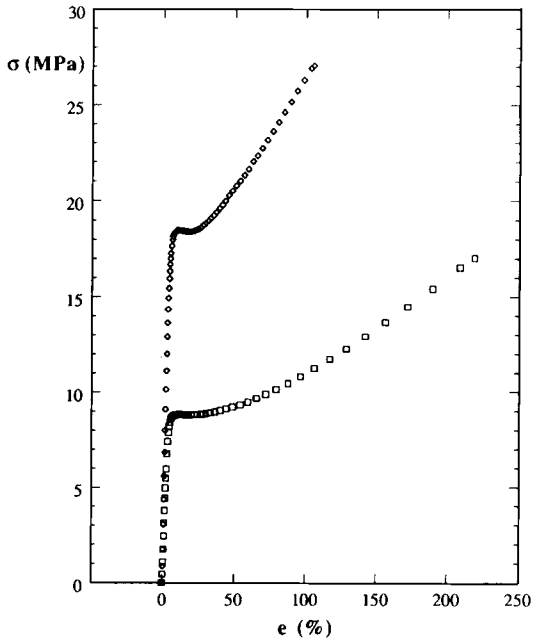

Figure 7 Representative stress–strain curves for H12MDI/MDECA (◇) and MDI/MDEA (□).

aly in the previously reported data[8] as both G' and E are of the same magnitude; depending on Poisson's ratio (~ 0.4 for these materials) E should be 2.5 to 3 times greater than G'. This is the case for the data reported here with the same G' values as before and tensile properties determined on a more precise instrument than that used previously.

There are two characteristic regions to the stress–strain curves. At low strains the materials have a high modulus and the slope of the stress–strain curve is very steep. The materials show either an intrinsic yield point or an extrinsic yield point (which may be determined using the Considere construction[38]). The yield point is followed by extensive post-yield drawing with little increase in the nominal stress. Bengston and coworkers[39] have interpreted similar stress–strain curves for analogous solution polymerized polyurethanes as being typical of cocontinuous materials with the initial part of the curve being the deformation and yielding of the continuous hard-segment phase whilst the post-yield drawing is deformation of the rubbery network phase.

The stress–strain curves in Figure 5 are those of materials with different urea-group densities. At the test-temperature of 25°C the modulus ranks in the order MDI/DETDA > TDI/DETDA > MDI/MDEA and this is in agreement with the dynamic mechanical data. MDI/DETDA and TDI/DETDA have intrinsic yield points whereas MDI/MDEA has only an extrinsic yield point. After the yield point TDI/DETDA breaks with a low tensile strength and elongation, this is a very brittle material with behavior typical of a low molecular weight organic glass. Conversely, the two materials with lower urea group density, MDI/DETDA and MDI/MDEA, show extensive, linear post-yield drawing with drawing moduli (the slope of the stress–strain curve) of 7 and 5 MPa respectively.

The effect of polyurea structure on the stress–strain curves of the copolyureas with similar urea-group densities is shown in Figure 6. The two DETDA containing materials have approximately the same Young's modulus whereas that of MDI/DMTDA is ~ 100 MPa lower, this is in good agreement with the dynamic mechanical data. All three materials have an intrinsic yield point and show extensive post-yield drawing. MDI/DMTDA has lower yield stress and yield strain values than MDI/DETDA and consequently the stress is lower during drawing. However the modulus during drawing for these linear materials is the same at 7 MPa and contrasts with the value of 12 MPa for the cross-linked LF168/DETDA material.

The stress–strain curves of polyureas with aromatic and aliphatic hard segments are compared in Figure 7. At the test temperature of 25°C the aliphatic material has a higher modulus than the analogous aromatic material and this is in good agreement with the dynamic mechanical data. As previously discussed MDI/MDEA has only an extrinsic yield point whereas H_{12}MDI/MDECA has an intrinsic yield point with ~ double the yield stress. Both materials show post-yield drawing, the aromatic material has a drawing modulus of 5 MPa and an elongation of 222% whereas the aliphatic material has a drawing modulus of 10 MPa and an elongation of 108%.

Fracture Mechanics Analysis

The RIM materials studied have a wide range of physical properties when one considers that they are all nominally 50 wt % rubber and 50 wt % glass; at one extreme TDI/DETDA has a modulus approaching 600 MPa and an ultimate elongation of 17% whereas MDI/MDEA has a modulus of ~ 200 MPa and an ultimate elongation of > 200%. Therefore, to characterize the absolute fracture properties of this wide spectrum of materials using well established fracture tests is not trivial. The theoretical basis of the experiments discussed here is well established and there are a number of good reviews[40,41] to which the reader is recommended.

The materials with high ultimate elongations may be treated as rubbers and their fracture behavior analyzed according to the tearing criteria of Rivlin and Thomas[42] to yield the "tearing energy" or more

precisely the critical strain energy release rate, G_c. The TDI/DETDA material is brittle and thus it's fracture behavior is amenable to analysis using the theories of linear elastic fracture mechanics, LEFM,[40] to yield the fracture toughness or more precisely the critical stress intensity factor, K_c. In an attempt to overcome the problems discussed above and make self-consistent measurements of the fracture behavior of RIM copolyureas, the single edge notch (SEN) technique was adopted and the tearing of rubber and/or the LEFM approach was used to analyze the experimental data.

During fracture testing of the more ductile materials, the instant of crack initiation is defined by Rivlin and Thomas[42] as the visible tearing associated with an increase in notch depth. This is a potential source of error as the onset of crack growth must be "eyeballed." However, within experimental error, two workers in our laboratory measured the same values of G_c for two different sets of materials. As detailed in the experimental section the load extension curves were converted into stress–strain curves and the energy required to propagate the crack, W_c, was obtained by integrating the area up to the onset of crack propagation. A typical set of force time curves are shown in Figure 8 as a function of crack length, a. The strain energy density at the onset of crack growth, W_c, has been defined for the sample with the longest crack length, the force–time data

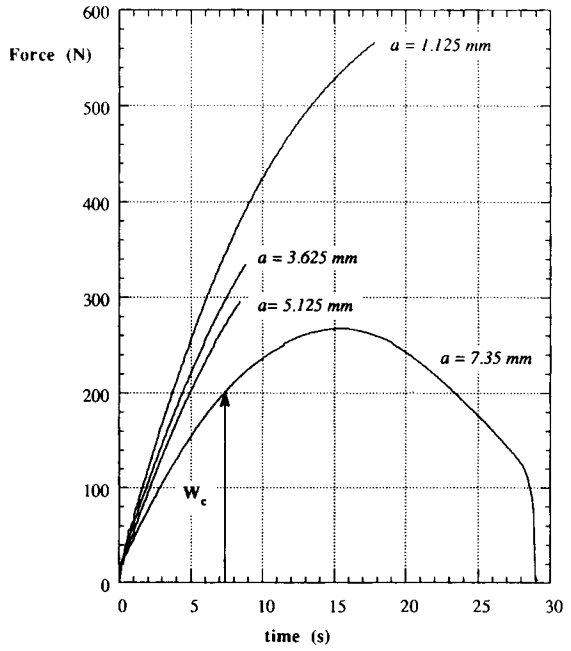

Figure 8 Typical force–time curves for MDI/DETDA specimens with different crack lengths, shown only to the point of crack propagation, with the exception of the lowermost curve which is complete.

up to the onset of crack growth only, is shown for the other speicmens. The critical strain energy release rate is defined, for this geometry, by the relation

$$G_c = 2kW_c a \tag{5}$$

where a is the original crack length; An approximate expression for k has been derived by Lake[43] where $k \simeq \pi/\lambda_c^{1/2}$ and λ_c is the extension ratio of the specimen at the onset of crack propagation. Hence, one can obtain G_c from the slope of a plot of $2kW_c$ vs. $1/a$ and a typical example of such a plot, for the MDI/ DETDA material, is shown in Figure 9. The $2kW_c$ vs. $1/a$ plots were linear and passed through the origin which is in good agreement with the prediction of fracture by tearing.[44] The analysis for G_c is dependent on the specimens being under conditions of plane-strain, that is, where the strain in one of the principal axes (the strain normal to the applied stress) is zero. According to Williams[40] the plane-strain criteria for SEN specimens of thickness b is

$$b > 2.5(K_c/\sigma_y)^2 \tag{6}$$

where σ_y is the yield stress. MDI/DETDA has an extrinsic yield stress of 19.6 MPa and a G_c value of 3.22 kJ m^2. Thus for the plane-strain criteria to be fulfilled the specimen must have a thickness of $b > 11.5$ mm. The RIM mold had a constant thickness of 3 mm and therefore the values of G_c determined experimentally will be overestimated (by up to a factor of 10^{40}). This will also be true of the K_c values calculated from measured G_c even though they have been calculated from the plane-stress equation

$$G_c = K_c^2/E \tag{7}$$

During testing of TDI/DETDA, the instant of crack propagation corresponded with a massive acceleration of the crack tip and brittle fracture of the specimens resulted in force deflection curves that were approximately triangular. The forces required to propagate the cracks were obtained from the maxima in the curves from which the values of remote stress to failure, σ_c, were calculated. From the values of σ_c and the corresponding initial crack depths, a, a plot of $\sigma_c^2 Y^2$ vs. $1/a$ was constructed according to

$$K_c^2 = \sigma_c^2 Y^2 a \tag{8}$$

where

$$Y = 1.99 - 0.41(a/d) + 18.70(a/d)^2 - 38.48(a/d)^3 + 53.85(a/d)^{4n} \tag{9}$$

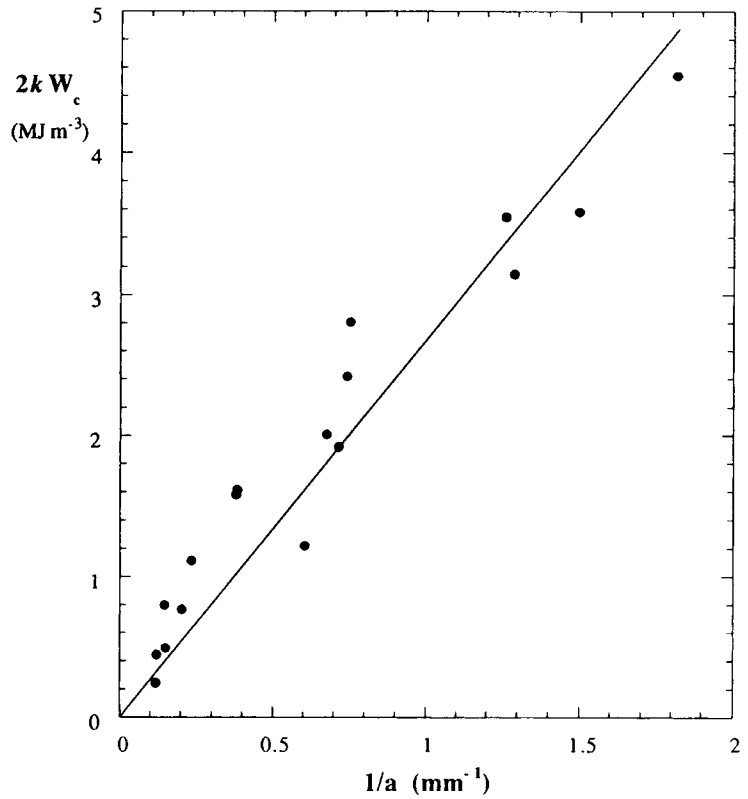

Figure 9 Typical $2kWc$ vs. $1/a$ plot for MDI/DETDA. A least squares linear fit to the data gives a slope, G_c = 2.68 kJ m^{-2} and a correlation coefficient of 0.97.

the shape factor for this specimen geometry.[40] The plot was linear and passed through the origin, with a correlation coefficient of 0.97 (a good set of data in terms of fracture experiments[41]), in agreement with LEFM. The analysis for K_c is also dependent on the specimens being under conditions of plane-strain. TDI/DETDA has an intrinsic yield stress of 15.9 MPa and a K_c value of 0.18 MPa m$^{1/2}$. Thus the plane-strain criteria was fulfilled as the specimen must have a minimum thickness of $b > 0.34$ mm.

The values of G_c, K_c and b for each of the copolyureas are presented in Table III. The fracture energy and fracture toughness have a strong dependency on urea group density as may be observed in the G_c and K_c data, whereas these properties are less sensitive to the fine structure of materials with similar urea group densities. The aliphatic material has lower fracture properties than its aromatic analog and this is most likely a function of its higher modulus and yield strength. Figure 10(a–c) presents scanning electron micrographs of the fracture surfaces, close to the original crack, for the materials with different urea group contents. The nature of the fracture process may be observed from the appearance of the fractured specimen. The surface of MDI/MDEA shows gross tearing and there is also a 50% reduction in the thickness of the specimen ahead of the notch. The reduction in cross section is due to stress concentration induced local yielding. The appearance of MDI/DETDA is very similar to MDI/MDEA with yielding and tearing, the cross-sectional area ahead of the notch being reduced to 70% of its original value. Both of these materials were tested under conditions approximating to plane stress and the amount of yielding correlates with magnitude of the unnotched yield stress, as previously observed by Ryan et al.[28] The micrograph of the stiffer and more brittle TDI/DETDA specimen is significantly different. Far ahead of the original crack the surface is smooth and almost featureless showing very little surface damage. However, there was much damage caused by the razor blade during notch formation and due to premature crack-growth the notch depths for this material are subject to errors. Also, because of the brittleness of this material the specimens were tested under conditions approximating to plane-strain and the specimen cross section does not show any reduction ahead of the notch.

DISCUSSION

The properties of copolyureas formed by RIM are dominated by their microphase morphology comprising rubbery, polyether soft segments end-linked with rigid, hydrogen-bonded polyurea hard segments. As discussed in the introduction, bulk copolymerization is equivalent to a thermodynamic quench from the homogeneous monomers in one-phase space to an unstable mixture of block copolymers and homopolymers in two-phase space and this causes a physical gelation in these linear systems. Recent experimental results indicate that spinodal decomposition, which is then arrested by the eventual vitrification of the hard segment, occurs to form materials with nonequilibrium, cocontinuous morphologies.[23,24] Thus the RIM process involves a kinetic competition between polymerization and microphase separation which may produce, at one extreme, a phase-separated mixture of polyurea and end-capped polyether with very few interphase covalent bonds or, at the other extreme, a microphase-separated block copolymer. The nonequilibrium structure formed will have some of the features of micro- and macrophase separation as at the onset of the ordering process the reacting mixture contains unreacted monomers, short hard segment sequences and, tri-, penta- . . . multiblock copolymers.

Effects of Urea-Group Density

The aromatic copolyureas with different urea-group densities show the greatest differences in materials properties. The size-scale of microphase separation decreases with increasing urea group content as can be seen from the d_1 spacing and chord length data in Table II. The same trend is also seen with the gel-time and these two phenomena are most likely related; a shorter physical gel-time implies a shorter time for diffusion and thus a finer nonequilibrium structure will be frozen in when the hard segment vitrifies. Despite the TDI/DETDA system having the shortest gel-time it is the polymer with the highest degree of microphase separation as shown by ΔC_p at T_g^s (see Table II) and the flatness of the modulus plateau (see Fig. 2). This results because the high concentration of urea groups endow this system with the greatest driving force to microphase separation, i.e., the greatest depth of quench in the phase diagram.[23,24] (The driving force to phase separation is proportional to the square of the difference in solubility parameter of the hard and soft segments.[24,48]) MDI/DETDA has a slightly longer gel-time than the TDI/DETDA system but its lower driving force to microphase separation means that the concentration gradients between the phases are less steep when vitrification occurs. Thus ΔC_p at T_g^s is smaller and there is a pronounced slope in G' as the mixed material relaxes. The slowest gelling material, MDI/MDEA also has the lowest driving force to microphase separation (the smallest solubility parameter difference) but as it has a longer microphase separation time it may achieve a structure that is closer to equilibrium. This explains why is has the same ΔC_p at T_g^s as MDI/DETDA but its modulus is less sensitive to temperature. It is only at high temperatures, between 200 and 250°C, that the modulus of these materials is dominated by urea group content. At temperatures below this, the modulus is dominated by the nonequilibrium structure, i.e., some portion of the soft segment is involved in glassy mixtures which increases the materials' stiffness. As the material involved in these compositional gradients becomes mobile and rubbery, microphase separation continues and each type of monomer segment will diffuse to its respective microphase. Thermal annealing causing improved microphase separation in analogous RIM copolyurea networks has been observed quite emphatically by Birch et al.[45] from the sharpening of transitions by DMA and increases in ΔC_p at T_g^s by DSC.

Tensile stress–strain studies show that TDI/DETDA is a very brittle material which has a yield point that immediately precedes fracture with no upturn in the stress. Conversely, MDI/DETDA and MDI/MDEA show extensive post-yield drawing with moduli that are dependent on the urea-group content. The initial part of the stress–strain curve is interpreted as deformation and yielding of the continuous hard segment microphase whereas the post-yield drawing is due to the deformation of the rubbery polyether microphase. The small-strain modulus of these materials is in agreement with that predicted by theories for cocontinuous morphologies[23,28,46] whilst the modulus during post-yield drawing is an order of magnitude greater than that of the equivalent polyether network.[47] Though there is a great deal of data available[4–12,15,16,18,23,25–27,36,39–43,45,47] to compare with the large-strain properties reported here there is no well-established theory to predict the ultimate properties of segmented block copolymers. The fracture measurements and the micrographs of fracture surfaces (Figs. 10–12) confirm the brittle nature of TDI/DETDA. Previous work by Willkomm et al.[8,11] showed that RIM copolyureas contained significant quantities of free hard segment and that these cause brittleness on demolding. We propose that this is a

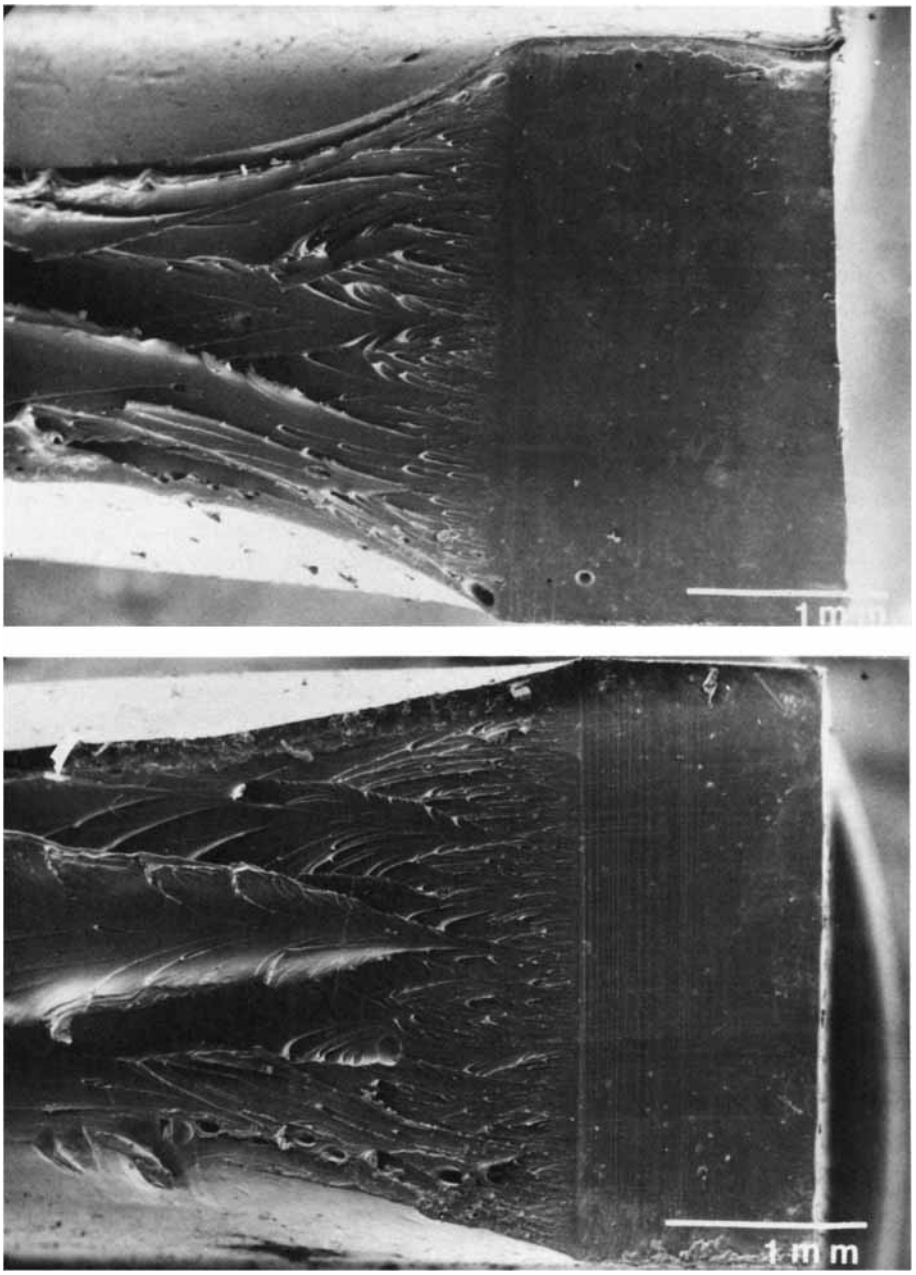

Figure 10 Scanning electron micrographs of copolyurea fracture surfaces, the direction of crack growth is from right to left. (a) MDI/MDEA; (b) MDI/DETDA; and (c) TDI/DETDA.

free-volume effect where microvoids associated with these isolated hard segments act as stress concentrators. Griffiths' hypothesis,[48] which relates the stress at failure to the intrinsic flaw size, ζ, and true surface energy of the material, γ, through

$$\sigma_c^2 \pi \zeta = 2\gamma E \qquad (10)$$

may be used to calculate an intrinsic flaw size from the ultimate stress as $2\gamma = G_c$ for perfectly brittle fracture. Thus TDI/DETDA has a large intrinsic flaw size of $\sim$ 40 μm. A similar calculation is not possible for the other two materials as G_c obviously encompasses energy dissipated in yielding. Despite the difference in the stress condition in these materials, the two orders of magnitude difference between the observed values of G_c for TDI/DETDA

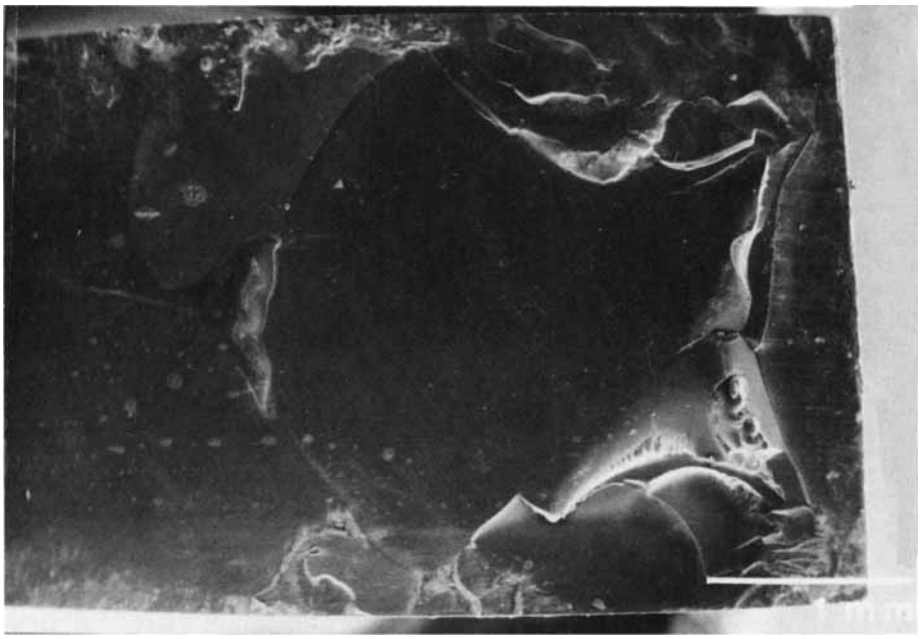

Figure 10 (*Continued from the previous page*)

and MDI/MDEA is far greater than difference between plane-stress and plane-strain values obtained for the same material.[41]

Effects of Crosslinking and Reaction Rate at Constant Urea-Group Density

LF168 is a modified version of MDI which contains ~ 15% of trifunctional material and the urea group contents, reaction rates, gel-times and microphase separation kinetics of materials made from these two monomers are similar. Thus the SAXS curves are virtually indistinguishable at low scattering vector and the materials have essentially the same degree of phase separation (from ΔC_p at T_g^s) and the same size scale. A corollary of this is that the small-strain properties of these materials are identical over a wide temperature interval. The divergence in dynamic mechanical properties above 200°C is most likely due to carbodiimide initiated degradation in LF168/DETDA. It is only at large strains or in the fracture behavior that we see the effect of such a low level of crosslinking. Thus, LF168/DETDA is much stiffer than MDI/DMTDA during post-yield drawing and has a higher tensile strength and fracture toughness.

DMTDA is structurally analogous to DETDA with thiomethyl groups replacing ethyl groups. This has three effects in terms of the polymerization, the amine groups are deactivated making the hard segment forming reaction slower, the hard segment formed has a higher density (and thus a lower hard segment volume fraction) and the replacement of a carbon with sulfur further increases the electron density difference between the phases. Due to its lower gel time but similar driving force to phase separation, MDI/DMTDA develops a coarser structure than MDI/DETDA, as indicated by the SAXS data, but has a similar degree of microphase separation as inferred from ΔC_p at T_g^s and the shape of the DMA curves. The lower modulus of this material, as observed by both DMA and stress–strain experiments, is due in part to its reduced hard segment volume fraction. However, the slope of the post-yield drawing is similar for both materials due to their identical soft segment structure. The fracture surfaces of these materials are indistinguishable and the increased G_c of MDI/DMTDA is due to its lower yield stress.

Aromatic Versus Aliphatic Hard Segments

H_{12}MDI/MDECA is the hydrogenated analog of MDI/MDEA. The aliphatic diamine is more reactive and the aliphatic diisocyanate is less reactive than the aromatic analog. Thus the reactivity differences work against each other and the gel-time of the aliphatic polyurea is only slightly longer than that of the aromatic polyurea. The aliphatic material appears to be more phase separated, T_g^s is lower, ΔC_p

at T_g^s is of greater magnitude and the peak in tan δ is sharper. Furthermore, it has a much smaller structure as indicated by the d_1 spacing in Table II. This is contrary to what we would expect as the aromatic material has a slightly greater driving force to phase separation (the hard segment solubility parameters calculated from molar group contribution data are 10.6 $cal^{1/2}$ $cm^{-3/2}$ for MDI/MDEA[48] and 9.5 $cal^{1/2}/cm^{-3/2}$ for H_{12}MDI/MDECA). One possible explanation is that the aromatic material is less mobile and has a higher T_g, thus as microphase separation occurs, larger regions with concentration gradients are frozen in by vitrification. Another unusual feature of these data is the higher modulus of the aliphatic copolyurea over a wide temperature interval (see Fig. 4) and its increased stress at all strains (see Fig. 7). Intuitively an aromatic polymer should be stiffer than its aliphatic analog, however, the moduli of these copolyureas are dominated by the volume fraction of glassy material. Ryan et al.[23,28] have shown similar copolymers to give a good fit to the modulus predicted[46] for a material with a cocontinuous structure. If we assume that both hard segments have the same glassy shear modulus of 2 GPa and the soft segment has a shear modulus of 1 MPa then we can predict the modulus of the composite from the volume fraction of hard segment through the Davies equation.[46]

$$G^{1/5} = \phi_{HS} G_{HS}^{1/5} + \phi_{SS} G_{SS}^{1/5} \qquad (11)$$

Thus shear moduli of 64 MPa and 46 MPa are predicted for H_{12}MDI/MDECA and MDI/MDEA respectively and these compare with G' measured at 100°C of 119 MPa and 65 MPa, respectively The fracture surfaces of these two materials look alike with gross yielding and tearing. The lower yield stress of MDI/MDEA is translated into a higher G_c value as more energy is dissipated by flow.

SUMMARY AND CONCLUSIONS

The size scale of copolyureas, determined by SAXS is related to both the speed of reaction (gel-time) and the driving force for microphase separation. RIM copolyureas have a nonequilibrium morphology and the degree of microphase separation may be related to the change in specific heat capacity at T_g^s in the manner of Camberlin and Pascault.[49] Small strain properties, E and G', are very sensitive to the volume fraction of glassy material. This is manifest as the temperature dependence of G' and accounts for the increased modulus of the aliphatic copolyurea when compared to the aromatic copolyurea. Large-strain properties are particularly sensitive to cross-linking. For the linear materials the magnitude of the ultimate properties depends on the detail of hard segment structure but the modulus during post-yield drawing is relatively structure independent. Cross-linked materials strain-harden more than the corresponding linear materials. The poor ultimate properties of TDI/DETDA may be due to its large intrinsic flaw size and show the deleterious effect of increasing the urea-group content.

Fracture studies allow us to characterize the materials further. In common with other engineering materials,[50] the magnitude of G_c is proportional to the yield stress, indicating that the fracture process is that of a continuum. Thus the material with the lowest yield stress, MDI/MDEA, has the greatest observed G_c value. This correlation does not apply to TDI/DETDA which is obviously (see Figure 10) very brittle which suggests a molecular origin for the brittleness of this polymer. The majority of the fracture mechanics measurements were made in conditions approximating to plane-stress. This does not give the limiting value of G_c and other techniques which allow determination of a plane-strain G_c in these limited thickness, ductile materials should be developed. However, the two orders of magnitude difference in G_c observed between TDI/DETDA and MDI/MDEA is astounding when one considers the materials are both nominally 50 wt % rubber and 50 wt % glass with moduli which differ by only a factor of three, and characterize an enormous difference in materials properties.

The authors would like to thank Edward Anderson for assistance with reaction injection molding and Chris Scott for the preparation of the micrographs. We are grateful to Dow Chemical, Ethyl Corporation, ICI Americas, Lonza AG, Mobay, and the Texaco Chemical Company for the kind donation of the chemical reactants. This work was supported in part by a NATO fellowship to AJR, the National Science Foundation, and the industrial sponsors of the University of Minnesota Polymerization and Polymer Process Engineering Center.

REFERENCES

1. C. W. Macosko, *RIM Fundamentals*, Hanser, Munich (1989).
2. R. E. Camargo, C. W. Macosko, M. Tirrell, and S. T. Wellinghof, *Polymer*, **26,** 1145 (1985).
3. W. P. Yang and C. W. Macosko, *Makromol. Chem. Makromol. Symp.*, **25,** 23 (1989).
4. R. B. Turner, *Polymer Composites*, **5,** 151 (1984).

5. D. Nissen and R. A. Markovs, *J. Elastomers Plast.*, **15,** 96 (1983).
6. A. J. Ryan, J. L. Stanford, and R. H. Still in *Integration of Polymer Science and Technology* 2nd ed., P. J. Lemstran and L. A. Kleintjens, Eds., Elsevier, London 1988, p. 515.
7. R. J. G. Dominguez, *J. Cell. Plast.*, **20,** 433 (1984).
8. W. R. Willkomm, Z. S. Chen, C. W. Macosko, D. A. Gobran, and E. L. Thomas, *Polym. Eng. and Sci.*, **28,** 888 (1988).
9. A. J. Ryan, J. L. Stanford, and A. N. Wilkinson, *Polym. Bull*, **18,** 517 (1987).
10. J. L. Stanford, A. N. Wilkinson, D.-K. Lee, and A. J. Ryan, *Plast. Rubb. Proc. Appl.*, **13,** 111 (1990).
11. W. R. Willkomm, Ph.D. Thesis, University of Minnesota (1990).
12. J. L. M. van der Loos and A. A. van Geneen, *ACS Symp. Series*, **270,** 181 (1985).
13. L. Leibler, *Macromolecules*, **13,** 1602 (1980).
14. G. H. Frederickson and E. Helfand, *J. Chem. Phys.* **87,** 697 (1987).
15. M. J. Folkes and A. Keller, in *The Physics of Glassy Polymers*, R. N. Haward, Ed., Wiley, New York, 1973, pp. 548–597.
16. M. J. Folkes, Ed., *Processing, Structure and Properties of Block Copolymers*, Elsevier, New York, 1985.
17. H. Benoit and G. Hadziioannou, *Macromolecules*, **21,** 1449 (1988).
18. C. H. Y. Chen-Tsai, E. L. Thomas, W. J. MacKnight, and N. S. Schneider, *Polymer*, **27,** 659 (1986).
19. C. Li, S. L. Goodman, R. M. Albrecht, and S. L. Cooper, *Macromolecules*, **21,** 2367 (1988).
20. S. L. Goodman, C. Li, S. L. Cooper, and R. M. Albrecht, Proc. 46th Ann. Meet. Electron Microscopy Society of America, San Francisco Press Inc., San Francisco, 1988, p. 936–937.
21. L. H. Peebles Jr., *Macromolecules*, **7,** 872, (1974); **9,** 58 (1976).
22. M. C. Pannone and C. W. Macosko, *J. Appl. Polym. Sci.*, **34,** 2409 (1987).
23. A. J. Ryan, J. L. Stanford, and R. H. Still, *Plast. Rubb. Proc. Appl.*, **13,** 99 (1990).
24. A. J. Ryan, *Polymer*, **31,** 707 (1989).
25. J. R. Dawson and J. B. Shortall, *Cellular Polymers*, **1,** 41 (1982).
26. N. Parvisi and J. B. Shortall, *Cellular Polymers*, **2,** 251 (1983).
27. J. L. Stanford, *AIChE Symp. Ser.*, **260(84),** 74 (1988).
28. A. J. Ryan, J. L. Stanford, and R. H. Still, *Polymer*, to appear.
29. D. W. Van Krevelen, *Properties of Polymers: Correlations with Chemical Structure*, 2nd Ed., Ch. 4, Elsevier, Amsterdam, 1972.
30. L. J. Lee and C. W. Macosko, *SPE ANTEC Tech. Pap.*, **24,** 151 (1978); K. Mikkelson and C. W. Macosko, *J. Cell. Plast.*, **21,** 29 (1989).
31. C. W. Macosko and D. B. McIntyre, U.S. Patent 4,473,531 (1984).
32. L. M. Leung and J. T. Koberstein, *J. Polym. Sci. Polym. Phys. Ed.*, **23,** 1883 (1985).
33. A. Galambos, PhD Thesis, Princeton University (1989).
34. P. Debye and A. M. Bueche, *J. Appl. Phys.*, **20,** 518 (1949).
35. P. Debye, H. R. Anderson Jr., and H. Brumberger Jr., *J. Appl. Phys.*, **28,** 679 (1957).
36. Z. S. Chen, W. P. Yang, and C. W. Macosko, *Rubb. Chem. Technol*, **61,** 86 (1988).
37. Y. Camberlin and J. P. Pascault, *J. Polym. Sci. Polym. Chem. Ed.*, **21,** 415 (1983).
38. I. M. Ward, *Mechanical Properties of Solid Polymers*, Wiley, London (1971).
39. B. Bengtson, C. Feger, W. J. MacKnight, and N. S. Schneider, *Polymer*, **26,** 895 (1985).
40. J. G. G. Williams, *Fracture Mechanics of Polymers*, Horwood, Chichester, UK (1984).
41. A. J. Kinloch and R. J. Young, *Fracture Behavior of Polymers*, Applied Science, London (1985).
42. R. S. Rivlin and A. G. Thomas, *J. Polym. Sci.*, **10,** 291 (1953).
43. G. J. Lake, *Yield, Deformation and Fracture in Polymers*, Conf. Proc. Physics Institute, London, 1970, p. 531.
44. H. W. Greensmiths, *J. Appl. Polym. Sci.*, **7,** 993 (1963).
45. A. J. Birch, J. L. Stanford, and A. J. Ryan, *Polym. Bull.*, **22,** 629 (1989).
46. W. E. Davies, *J. Phys. D. Appl. Phys.*, **161,** 318 (1971); **161,** 1176 (1971); **161,** 1325 (1971).
47. D.-K. Lee, PhD Thesis, Victoria University of Manchester (1988).
48. A. J. Ryan, J. L. Stanford, and R. H. Still, *Polymer Commun.*, **29,** 196 (1988).
49. Y. Camberlin, J. P. Pascault, *J. Polym. Sci. Polym. Chem. Ed.*, **27,** 415 (1983).
50. R. W. Herzberg, *Deformation and Fracture Mechanics of Engineering Materials*, Wiley, New York, 1976.

Received February 21, 1990
Accepted March 13, 1990